Journal of Oceanology and Limnology
Vol. 38 No. 5, P. 1476-1487, 2020
https://doi.org/10.1007/s00343-020-0045-2

Calcium isotopic signatures of depleted mid-ocean ridge basalts from the northeastern Pacific*

ZHU Hongli[1, 2, 3], DU Long[4, **], ZHANG Zhaofeng[5], SUN Weidong[1, 2, 3, 6]

[1] *Center of Deep Sea Research, Institute of Oceanography, Chinese Academy of Sciences, Qingdao 266071, China*
[2] *Laboratory for Marine Mineral Resources, Pilot National Laboratory for Marine Science and Technology (Qingdao), Qingdao 266237, China*
[3] *Center for Ocean Mega-Science, Chinese Academy of Sciences, Qingdao 266071, China*
[4] *College of Earth Science and Engineering, Shandong University of Science and Technology, Qingdao 266590, China*
[5] *State Key Laboratory of Isotope Geochemistry, Guangzhou Institute of Geochemistry, Chinese Academy of Sciences, Guangzhou 510640, China*
[6] *University of Chinese Academy of Sciences, Beijing 100049, China*

Received Jan. 19, 2020; accepted in principle Mar. 9, 2020; accepted for publication Mar. 25, 2020

Abstract A number of high-temperature processes (e.g., melt-rock reactions, metasomatism, partial melting) can produce significant Ca isotopic fractionation and heterogeneity in the mantle, but the mechanism for such fractionation remains obscure. To investigate the effect of mantle partial melting on Ca isotopic fractionation, we reported high-precision Ca isotopic compositions of depleted mid-ocean ridge basalts (MORBs) from the East Pacific Rise and Ecuador Rift in the northeastern Pacific. The $\delta^{44/40}$Ca of these MORB samples exhibit a narrow variation from 0.84‰ to 0.88‰ with an average of 0.85‰±0.03‰, which are similar to those of reported MORBs (0.83‰±0.11‰) and back-arc basin basalts (BABBs, 0.80‰±0.08‰) in literature, but are lower than the estimate value for the bulk silicate Earth (BSE, 0.94‰±0.05‰). The low $\delta^{44/40}$Ca signatures of MORB samples in this study cannot be caused by fractional crystallization, since intermediate-mafic differentiation has been demonstrated having only limited effects on Ca isotopic fractionation. Instead, the offset of $\delta^{44/40}$Ca between MORBs and the BSE is most likely produced by mantle partial melting. During this process, the light Ca isotopes are preferentially transferred to the melt, while the heavy ones tend to stay in the residue, which is consistent with the fact that $\delta^{44/40}$Ca of melt-depleted peridotites increases with partial melting in literature. The behavior of Ca isotopes during mantle partial melting is closely related to the inter-mineral (Cpx and Opx) Ca isotopic fractionation and melting mineral modes. Mantle partial melting is one of the common processes that can induce lower $\delta^{44/40}$Ca values in basalts and Ca isotopic heterogeneity in Earth's mantle.

Keyword: Ca isotopes; mid-ocean ridge basalts (MORBs); mantle partial melting; magma differentiation

1 INTRODUCTION

Calcium is one of the major elements in the Earth and has six stable isotopes (^{40}Ca, ^{42}Ca, ^{43}Ca, ^{44}Ca, ^{46}Ca, and ^{48}Ca) in nature (DePaolo, 2004). Except H and He, Ca has the largest relative mass difference ($\Delta m/m$=20%), which enables Ca to be an important geochemical and cosmochemical tracer (DePaolo, 2004). Calcium isotope ratios are commonly expressed in δ-notation relative to the standard NIST SRM 915a, e.g. $\delta^{44/40}\mathrm{Ca}\ (‰)=[(^{44}\mathrm{Ca}/^{40}\mathrm{Ca})_{\mathrm{sample}}/(^{44}\mathrm{Ca}/^{40}\mathrm{Ca})_{\mathrm{NIST\text{-}SRM\text{-}915a}}-1]\times 1\,000$. With the rapid improvements of analytical techniques, the accuracy and precision for the measurement of Ca isotopes have been greatly improved in the last two decades

* Supported by the National Natural Science Foundation of China (Nos. 41773009, 41873002), the Stake Key Laboratory of Geological Processes and Mineral Resources (No. GPMR201708), the National Science Foundation for Post-doctoral Scientists of China (No. 2018M640660), the Taishan Scholar Program of Shandong (No. TS201712075), and the AoShan Talents Cultivation Program Supported by Qingdao National Laboratory for Marine Science and Technology (No. 2017ASTCP-OS07)
** Corresponding author: dulong88@aliyun.com

(DePaolo, 2004; Fantle and Tipper, 2014). Calcium isotopes have been widely applied to biochemical (e.g., Farkaš et al., 2007a, b; Fantle and Tipper, 2014) and geological processes (e.g., Huang and Jacobsen, 2017; Lu et al., 2019; Wang et al., 2019; Dai et al., 2020; Wu et al., 2020; Zhu et al., 2020b).

To date, exploratory studies on Ca isotopes in igneous rocks mainly aim at constraining the Ca isotopic compositions of the bulk silicate Earth (BSE; Skulan et al., 1997; Huang et al., 2010; Simon and DePaolo, 2010; Amsellem et al., 2017; Kang et al., 2017; Chen et al., 2019b) and the mechanism of Ca isotopic fractionation during high-temperature processes (Huang et al., 2011; Chen et al., 2019a; Ionov et al., 2019; Lu et al., 2019; Wang et al., 2019). Initially, based on volcanic rocks and minerals in mantle peridotites, previous studies estimated the $\delta^{44/40}$Ca value for the BSE varies from 0.82‰ to 1.05‰ (Skulan et al., 1997; Huang et al., 2010; Simon and DePaolo, 2010). Nevertheless, due to the significant $\delta^{44/40}$Ca variation in volcanic rocks and inter-mineral Ca isotopic fractionation in mantle peridotites, a substantially larger number of well-selected samples should be analyzed to better characterize the Ca isotopic composition of the BSE. Kang et al. (2017) thereby analyzed 14 fertile peridotites without significant modification by metasomatism or partial melting and estimated $\delta^{44/40}$Ca of the BSE to be 0.94‰±0.05‰. Lherzolites from Balmuccia and Baldissero peridotite massifs were observed to have homogeneous $\delta^{44/40}$Ca values with an average of 0.94‰±0.11‰ (Chen et al., 2019b). Moreover, mantle pyroxenites and komatiites also show limited variations in Ca isotopic compositions with the mean $\delta^{44/40}$Ca of 0.92‰±0.16‰ and 0.90‰±0.05‰, respectively (Amsellem et al., 2019; Dai et al., 2020). The similar $\delta^{44/40}$Ca of fertile lherzolites, pyroxenites and komatiites from variable geological settings argue for that the value of 0.94‰ for the BSE can be considered robust (Kang et al., 2017; Amsellem et al., 2019; Chen et al., 2019b; Dai et al., 2020).

About 2‰ variation in $\delta^{44/40}$Ca has been documented in volcanic rocks, mantle xenoliths and their minerals (e.g., Amini et al., 2009; Liu et al., 2017a; Zhao et al., 2017; Ionov et al., 2019; Wang et al., 2019). This obvious Ca isotopic fractionation is closely related to several processes: (1) equilibrium and kinetic fractionation between minerals (Huang et al., 2010; Feng et al., 2014; Wang et al., 2017, 2019; Antonelli et al., 2019a, b); (2) kinetic isotopic fractionation driven by melt-rock reactions or metasomatism (Richter et al., 2009; Zhao et al., 2017; Chen et al., 2018); (3) mantle metasomatism by carbonate-rich melts/fluids derived from recycled marine carbonates and silicate-rich melts derived from eclogite (Huang et al., 2011; Kang et al., 2016, 2017, 2019; Liu et al., 2017a; Ionov et al., 2019); (4) melt extraction or partial melting (Zhu et al., 2018b, 2020a; Chen et al., 2019a, b; Ionov et al., 2019).

Recently, several lines of evidence suggest that mantle partial melting can induce distinguishable Ca isotopic fractionation and cause Ca isotopic heterogeneity in the mantle (Kang et al., 2017; Zhu et al., 2018b, 2020a; Chen et al., 2019a, b; Ionov et al., 2019). For example, strongly melt-depleted peridotites at 25%–30% melting are observed to have 0.1‰–0.2‰ higher $\delta^{44/40}$Ca values than those of fertile peridotites (Kang et al., 2017; Ionov et al., 2019). Accordingly, $\delta^{44/40}$Ca values of mid-ocean ridge basalts (MORBs) from the southern Juan de Fuca (JdF) Ridge, the East Pacific Rise (EPR) and the South Mid-Atlantic Ridge (SMAR) range from 0.75‰ to 0.94‰ with an average of 0.83‰±0.11‰ (2SD, N=21; Zhu et al., 2018b; Chen et al., 2019a), which are lower than those of their mantle source. Similarly, Zhu et al. (2020a) observed that $\delta^{44/40}$Ca values of back-arc basin basalts (BABBs) from the southwestern Pacific exhibit a narrow range from 0.73‰ to 0.89‰ with an average of 0.80‰±0.08‰ (2SD, N=21). They found that there is no systematic variation of $\delta^{44/40}$Ca with indicators of subduction contributions, and thus proposed that the offset of $\delta^{44/40}$Ca (~0.14‰) between the mantle and BABBs should be primarily controlled by Ca isotopic fractionation during partial melting (Zhu et al., 2020a). However, based on model simulations, Zhang et al. (2018) proposed that partial melting can produce significant effects on $\delta^{44/40}$Ca of melting residues (up to 0.3‰), but negligible effects on $\delta^{44/40}$Ca of the melts (<0.07‰).

To better understand the behavior of Ca isotopes during partial melting and constrain the extent of Ca isotopic fractionation during this process, here we present high-precision Ca isotopic compositions of a suit of fresh MORB samples from the northern East Pacific Rise and Ecuador Rift in the northeastern Pacific. Based on the data set for Ca stable isotopes in MORBs and reported mantle peridotites, we also perform model calculations to further assess the effects of partial melting on $\delta^{44/40}$Ca of melts and residues.

2 GEOLOGICAL SETTING AND SAMPLE

Fresh MORB samples from the northern EPR and Ecuador Rift in the northeastern Pacific were analysis in this study. The Ecuador Rift is located east of the Galapagos Spreading Center (Perfit et al., 1983). Samples from this rift represent a relatively primitive and depleted variety of N-MORB (Perfit et al., 1983). The EPR is a fast-spreading ridge (>80 mm/a) and has a voluminous basaltic production rate (Chen et al., 2019a). Based on trace element patterns, MORB samples from the EPR vary from rare incompatible element enriched MORB (E-MORB), typical normal MORB (N-MORB), to strong incompatible element depleted MORB (D-MORB) (Lundstrom et al., 1999; Sun et al., 2003). Data based on U-series disequilibria indicate that D-MORB from the northern EPR lack ^{230}Th excess, have high excesses of ^{226}Ra and ^{231}Pa, and resemble experimentally determined melts of peridotite at 1 GPa, implying derivation from relatively shallow level melting of spinel lherzolite at low residual porosity (Lundstrom et al., 1999). A recent study has presented Ca isotopic compositions of 8 MORB samples from the southern EPR (3°7′S; Chen et al., 2019a). Here, MORB samples from the northern EPR were recovered from the 9°N–10°N segment using the submersible ALVIN.

Our studied MORB samples from both the EPR and Ecuador Rift were previously investigated for Re and other trace element analysis by Sun et al. (2003) and classified as D-MORB. Note that they would generally be considered to be variations of N-type MORB and are not the extremely depleted types reported from other locations, e.g. some near axis seamounts and transform faults (Sun et al., 2003). These samples are fresh glasses with less than 2% phenocrysts or vesicles. Analyzed glasses were carefully handpicked under a binocular microscope to avoid visible phenocrysts and any alteration in appearance.

3 ANALYTICAL METHOD

Major and trace element concentrations of MORB samples were measured by Sun et al. (2003) using a JEOL6400 electron microscope and laser ablation inductively coupled plasma mass spectrometry (LA-ICP-MS) system, respectively. These MORB samples were selected from previous prepared glass separates (Sun et al., 2003) for Sr, Nd, and Ca isotope analysis.

3.1 Strontium and neodymium isotopic compositions

Fresh glasses were washed ultrasonically in ~1 mol/L HCl for 15 min and MQ water for 30 min. These glasses were grounded into 200 mesh power in an agate mortar. About 80 mg of sample powers were dissolved in Teflon beakers with a mixture of concentrated HF and HNO_3. After heating on a hotplate at 120°C for 5 d, these samples were dried down at 100°C. Then they were treated with 6 mol/L HCl several times until transparent solutions were obtained for Sr, Nd and Ca isotopic analysis.

Column chemistry for Sr and Nd isotopes were performed in a class 100 laboratory at the State Key Laboratory of Isotope Geochemistry (SKLaBIG), Guangzhou Institute of Geochemistry (GIG), Chinese Academy of Science (CAS) following the procedure described in Ma et al. (2013) and Du et al. (2018, 2019a, b). Strontium was purified on a column filled with 0.25 mL of Sr Spec resin. The purified Sr solutions were dried down and then were determined for Sr isotopic compositions on a Triton thermal ionization mass- spectrometer (TIMS) at SKLabIG, GIG, CAS. Neodymium was purified chromatographically according to a two-column procedure. The Nd isotopic compositions were measured on a Neptune Plus multi-collector inductively coupled plasma mass spectrometry (MC-ICP-MS) in the CAS Key Laboratory of Crust-Mantle Materials and Environment at the University of Science and Technology of China. The ^{87}Sr/^{86}Sr of NBS-987 and BCR-2 measured in the same analytical campaign were 0.710 245±0.000 009 (2SD, n=11) and 0.705 003±0.000 012 (2SD, n=3), respectively. The ^{143}Nd/^{144}Nd of JNdi and BCR-2 yielded 0.512 115±0.000 008 (2SD, n=9) and 0.512 632±0.000 011 (2SD, n=3), respectively. All these results for reference materials were in agreement with published data (e.g., Thirlwall, 1991; Tanaka et al., 2000; Raczek et al., 2003; Charlier et al., 2006).

3.2 Calcium isotopic compositions

Column chemistry and instrumental analysis for Ca isotopes were performed at SKLabIG, GIG, CAS, following the procedure described in Zhu et al. (2016, 2018a) and Liu et al. (2017b, 2019, 2020). Briefly, an aliquot of sample solution with 50 μg of Ca was mixed with 0.3 g of ^{42}Ca-^{43}Ca double spike solution that contained 8 μg of Ca. This mixture was dried down and dissolved in 0.05 mL of 1.6 mol/L HCl for

Table 1 Calcium, Sr and Nd isotopic compositions of studied MORB samples and standards

	SiO_2 (wt.%)	MgO (wt.%)	CaO (wt.%)	$(La/Sm)_N$	Eu/Eu*	$\delta^{44/40}Ca$ 1[a]	2	3	Mean	2SD[b]	2SE[c]	n[d]	$^{87}Sr/^{86}Sr$[e]	$^{143}Nd/^{144}Nd$[e]
East Pacific Rise														
Alv1558	49.88	8.71	13.04	0.36	1.06	0.85	0.80	0.85	0.84	0.06	0.03	3	0.702 394	0.513 247
Alv1566	50.33	7.95	12.99	0.38	0.99	0.89	0.87	0.79	0.85	0.10	0.06	3	0.702 430	0.513 224
Ecuador Rift														
1121-1	50.87	8.52	12.44	0.33	1.02	0.85	0.88	0.92	0.88	0.07	0.04	3	0.702 504	0.513 179
1123-2	50.70	8.09	12.65	0.35	0.98	0.87	0.85	0.81	0.84	0.06	0.04	3	0.702 619	0.513 138
1125-3	51.39	8.01	12.79			0.89	0.80	0.83	0.84	0.09	0.05	3	0.702 535	0.513 172
Standards														
NIST SRM 915a									-0.01	0.11	0.02	26		
IAPSO seawater									1.84	0.11	0.03	10		
BCR-2									0.83	0.09	0.04	5	0.705 003	0.512 632
NBS-987													0.710 245	
JNdi-1														0.512 115

[a] The number (1 to 3) represent replicate analyses of Ca isotopes from the same solution; [b] 2SD: two standard deviation; [c] 2SE: two standard deviation of the mean. 2SE=2SD/sqrt (n); [d] n: number of replicate analyses of Ca isotopes; [e] External reproducibilities (2SD) for $^{87}Sr/^{86}Sr$ and $^{143}Nd/^{144}Nd$ are better than 0.000 019 and 0.000 012, while in-run errors for $^{87}Sr/^{86}Sr$ and $^{143}Nd/^{144}Nd$ are better than 0.000 008 and 0.000 009, respectively.

Ca purification. The spiked sample solution was loaded onto a column filled with 1 mL of AG MP-50 (100–200 mesh) resin and eluted with 1.6 mol/L HCl. The Ca yield through the column chemistry were greater than 99%. To monitor the reproducibility and quality, one reference material and blank were processed as unknow samples. The blank was less than 70 ng and negligible compared to the amount of Ca loaded onto the column.

Calcium isotopic compositions were measured on a Triton TIMS. The ^{41}K was measured to evaluate the isobaric interference of ^{40}K on ^{40}Ca, and online correction was carried out using $^{40}K/^{41}K=1.738\,4\times10^{-3}$ (Heuser et al., 2002). Instrumental fractionation was corrected with a ^{42}Ca-^{43}Ca double spike technique (Heuser et al., 2002). All the Ca isotope data were reported as $\delta^{44/40}Ca$ relative to NIST SRM 915a. Each sample was analyzed 3 times using the same purified Ca cut. The analytical uncertainties of both two standard deviation (2SD) and two standard deviation of the mean (2SE) are listed in Table 1. The $\delta^{44/40}Ca$ values of NIST SRM 915a, IAPSO seawater and BCR-2 measured in the same session were -0.01‰±0.11‰ (2SD, n=26), 1.84‰±0.11‰ (2SD, n=10) and 0.83‰±0.09‰ (2SD, n=5), respectively, which were consistent with previous studies within error (e.g., Huang et al., 2010; Valdes et al., 2014; Feng et al., 2017, 2018; He et al., 2017; Li et al., 2018).

4 RESULT

Calcium, Sr, and Nd isotopic compositions of MORB samples from the northeastern Pacific are listed in Table 1. Major and trace element concentrations adopted from Sun et al. (2003) are listed in Supplementary Table S1.

In N-MORB normalized (Sun and McDonough, 1989) trace element abundance diagram (Fig.1a), MORB samples in this study are strongly depleted in incompatible elements and have slightly positive Pb anomalies. In the chondrite-normalized diagram (Fig.1b), these samples show strong light rare earth element (LREE) depletion. Based on $(La/Sm)_N$ ratios (0.3–0.4; Table 1), these samples are thereby classified into D-MORB type (Gale et al., 2013). The Sr and Nd isotopic compositions of these MORB samples are similar to those of the depleted MORB mantle (Workman and Hart, 2005), with $^{87}Sr/^{86}Sr$ ranging from 0.702 394 to 0.702 619 and $^{143}Nd/^{144}Nd$ ranging from 0.513 138 to 0.513 247 (Fig.2). As shown in Fig.3, the Ca isotopic compositions of these MORB samples display a narrow variation, with $\delta^{44/40}Ca$ ranging from 0.84‰ to 0.88‰, which overlaps the $\delta^{44/40}Ca$ range in reported MORBs (0.75‰–0.94‰; Zhu et al., 2018b; Chen et al., 2019a) and BABBs (0.73‰–0.89‰; Zhu et al., 2020a). Moreover, their average $\delta^{44/40}Ca$ (0.85‰±0.03‰; 2SD, N=5) is similar to the averages of reported MORBs (0.83‰±0.11‰;

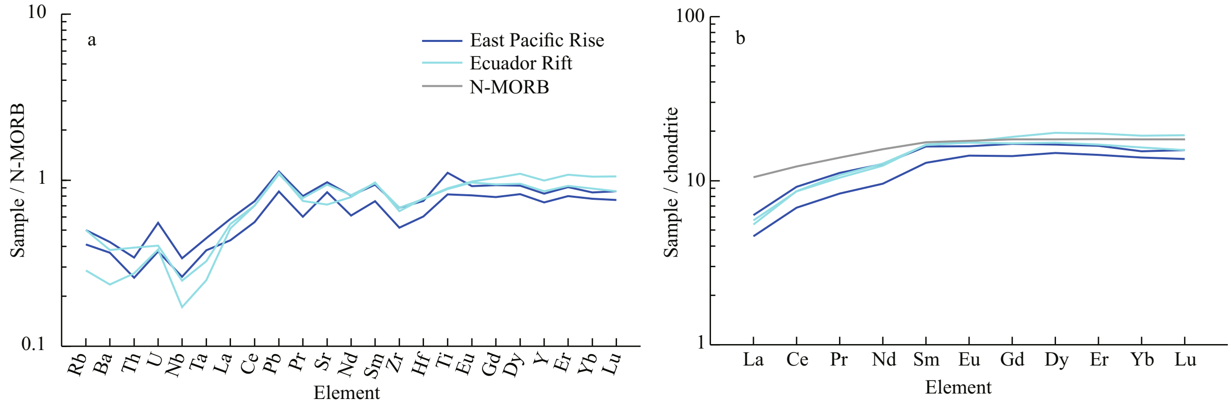

Fig.1 N-MORB normalized trace element patterns (a) and chondrite-normalized REE patterns of MORB samples (b) from the northeastern Pacific

N-MORB and chondrite normalizing values are from Sun and McDonough (1989).

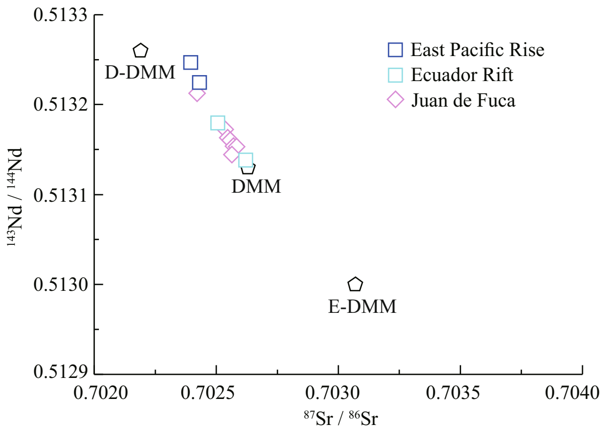

Fig.2 The $^{87}Sr/^{86}Sr$ versus $^{143}Nd/^{144}Nd$ of MORB samples investigated here

The $^{87}Sr/^{86}Sr$ and $^{143}Nd/^{144}Nd$ of D-DMM, DMM and E-DMM (hollow pentagons) are adopted from Workman and Hart (2005). Other N-MORB samples from the southern JdF Ridge (Zhu et al., 2018b) are shown for comparison. DMM=depleted MORB mantle.

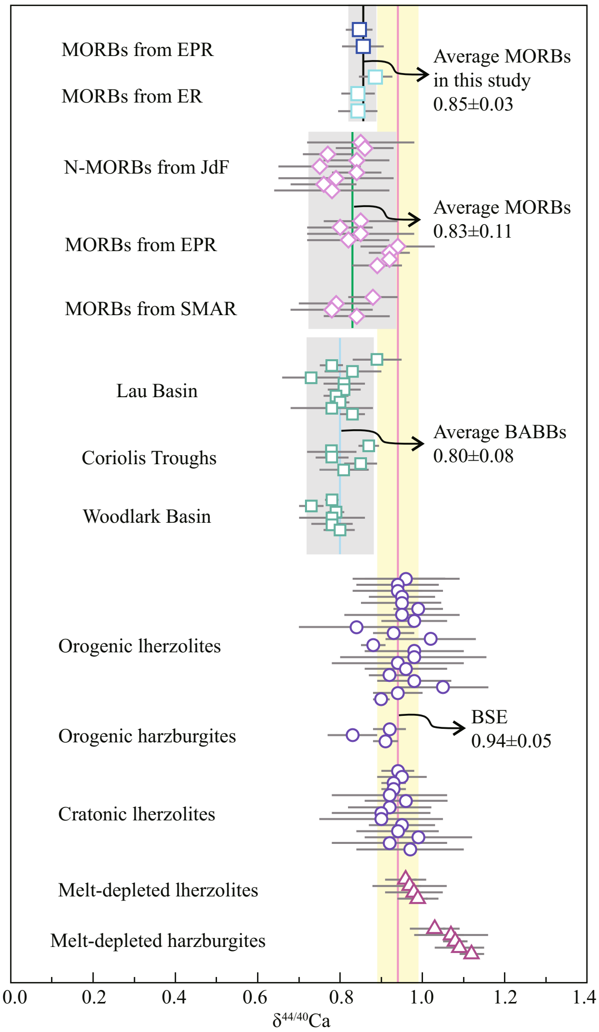

Fig.3 The $\delta^{44/40}$Ca values of studied MORB samples from the northeastern Pacific

MORB samples from the southern JdF Ridge, EPR and SMAR (Zhu et al., 2018b; Chen et al., 2019a), BABB samples from the southwestern Pacific (Zhu et al., 2020a) and peridotites (Kang et al., 2017; Chen et al., 2019b; Ionov et al., 2019) are shown for comparison. The pink vertical line and yellow bar represent the estimated $\delta^{44/40}$Ca value for the BSE (0.94‰±0.05‰; Kang et al., 2017).

2SD, N=21; Zhu et al., 2018b; Chen et al., 2019a) and BABBs (0.80‰±0.08‰; 2SD, N=21; Zhu et al., 2020a) (Fig.3).

5 DISCUSSION

5.1 The offset of $\delta^{44/40}$Ca between MORBs and their mantle source

Compared to N-MORB, MORB samples in this study are depleted in incompatible trace elements and LREE (Fig.1). Their Sr and Nd isotopic compositions vary from the depleted MORB mantle (DMM, the average for MORBs far from plumes) to the D-DMM (2σ depleted over the average for MORBs far from plumes) (Fig.2; Workman and Hart, 2005). All these geochemical characteristics suggest that these MORB samples were derived from the DMM without any mantle metasomatism.

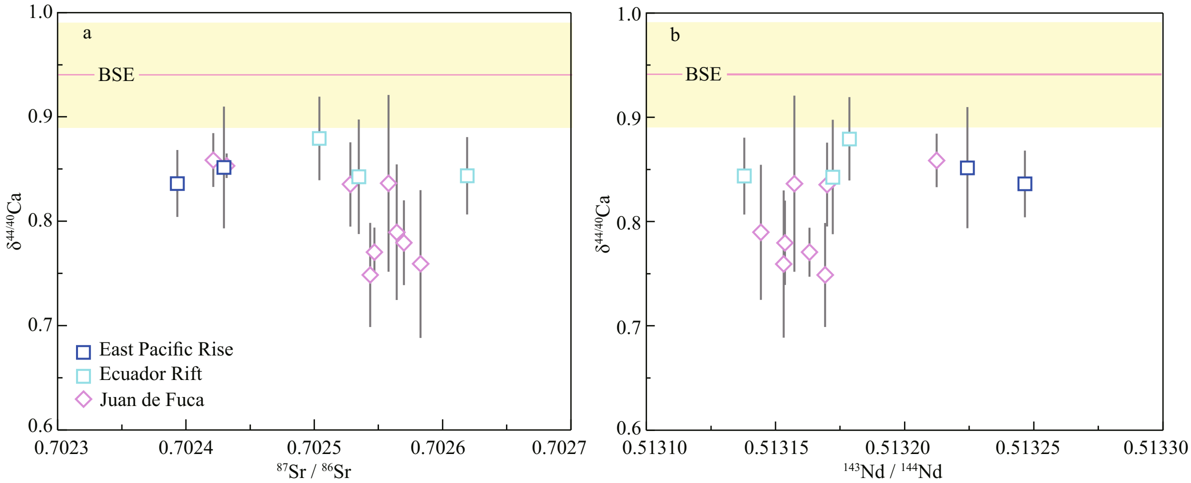

Fig.4 The $\delta^{44/40}$Ca versus $^{87}Sr/^{86}Sr$ (a) and $^{143}Nd/^{144}Nd$ (b) of studied MORB samples

N-MORB samples from the southern JdF Ridge (Zhu et al., 2018b) are shown for comparison. The pink vertical line and yellow bar represent the estimated $\delta^{44/40}$Ca value for the BSE (0.94‰±0.05‰; Kang et al., 2017).

Compared to the primitive mantle or BSE, the DMM has been depleted by low degree (2%–3%) of melt extraction (Salters and Stracke, 2004; Workman and Hart, 2005). The $\delta^{44/40}$Ca values (0.97‰–0.98‰) of moderately melt-depleted lherzolites at <20% melting are near the upper limit of the fertile peridotites (0.90‰–0.99‰) that without modification by melt extraction or metasomatism, suggesting low to moderate degrees of melt extraction cannot cause significant Ca isotopic fractionation in the residues (Kang et al., 2017; Chen et al., 2019b). Therefore, the $\delta^{44/40}$Ca of DMM maybe slightly higher than that of the BSE, but cannot be distinguished under the current analytical uncertainty of ~0.10‰ (Zhu et al., 2020a).

The $\delta^{44/40}$Ca values of studied MORB samples range from 0.84‰ to 0.88‰ with an average of 0.85‰±0.03‰ (2SD, N=5), which is ~0.10‰ lower than those of the BSE and DMM (Fig.4). Based on the calculation by Fantle and Tipper (2014), the effect of radiogenic ^{40}Ca ingrowth from ^{40}K decay on $\delta^{44/40}$Ca of these MORBs should be negligible, as these samples have quite low K/Ca ratios (<0.012) and young ages. A number of geological processes may cause the offset of $\delta^{44/40}$Ca between our studied MORB samples and their mantle source, including seawater and hydrothermal alteration (John et al., 2012; Blättler and Higgins, 2017; Chen et al., 2019a), fractional crystallization during magma differentiation (Zhang et al., 2018; Valdes et al., 2019), and mantle partial melting (Kang et al., 2017; Zhu et al., 2018b, 2020a; Chen et al., 2019a, b; Ionov et al., 2019). Below, we discuss the effects of these processed on the Ca isotopic budget of MORBs from the northeastern Pacific.

5.2 The effect of seawater and hydrothermal alteration

After eruption, MORB samples can experience seawater and hydrothermal alteration. Amini et al. (2008) found that the hydrothermal fluid endmember at the Lagotchev Field has a $\delta^{44/40}$Ca value of 0.91‰ (after renormalization to $\delta^{44/40}Ca_{seawater}$=1.86‰), which is near the upper limit of fresh MORBs but slightly higher than the average of fresh MORBs. With hydrothermal alteration, most of altered MORBs and an altered gabbroic rock are observed to have similar or slightly higher $\delta^{44/40}$Ca values than fresh MORBs and gabbroic rocks (John et al., 2012; Chen et al., 2019a). Moreover, the majority of hydrothermal carbonate veins which are formed as secondary minerals in altered oceanic crust (0.88‰–1.28‰) are conformed to be higher than the average of fresh MORBs (Blättler and Higgins, 2017). Therefore, seawater and hydrothermal alteration may induce limited Ca isotopic fractionation or slightly heavy Ca isotopic compositions in altered MORBs and altered oceanic crust.

In this study, fresh MORB glasses were handpicked under a binocular microscope to avoid any alteration in appearance. Several lines of evidence also support that these samples did not experience any alteration. First, these MORB samples did not show enrichments of large ion lithophile elements (LILE; Fig.1a). Secondly, they have lower $^{87}Sr/^{86}Sr$ values than the DMM (Fig.2). If these samples were influenced by seawater and hydrothermal alteration, they should show enrichments of LILE and have higher $^{87}Sr/^{86}Sr$ values than the DMM (Verma, 1992). Thus, seawater and hydrothermal alteration cannot account for the low $\delta^{44/40}$Ca signatures of our studied MORB samples.

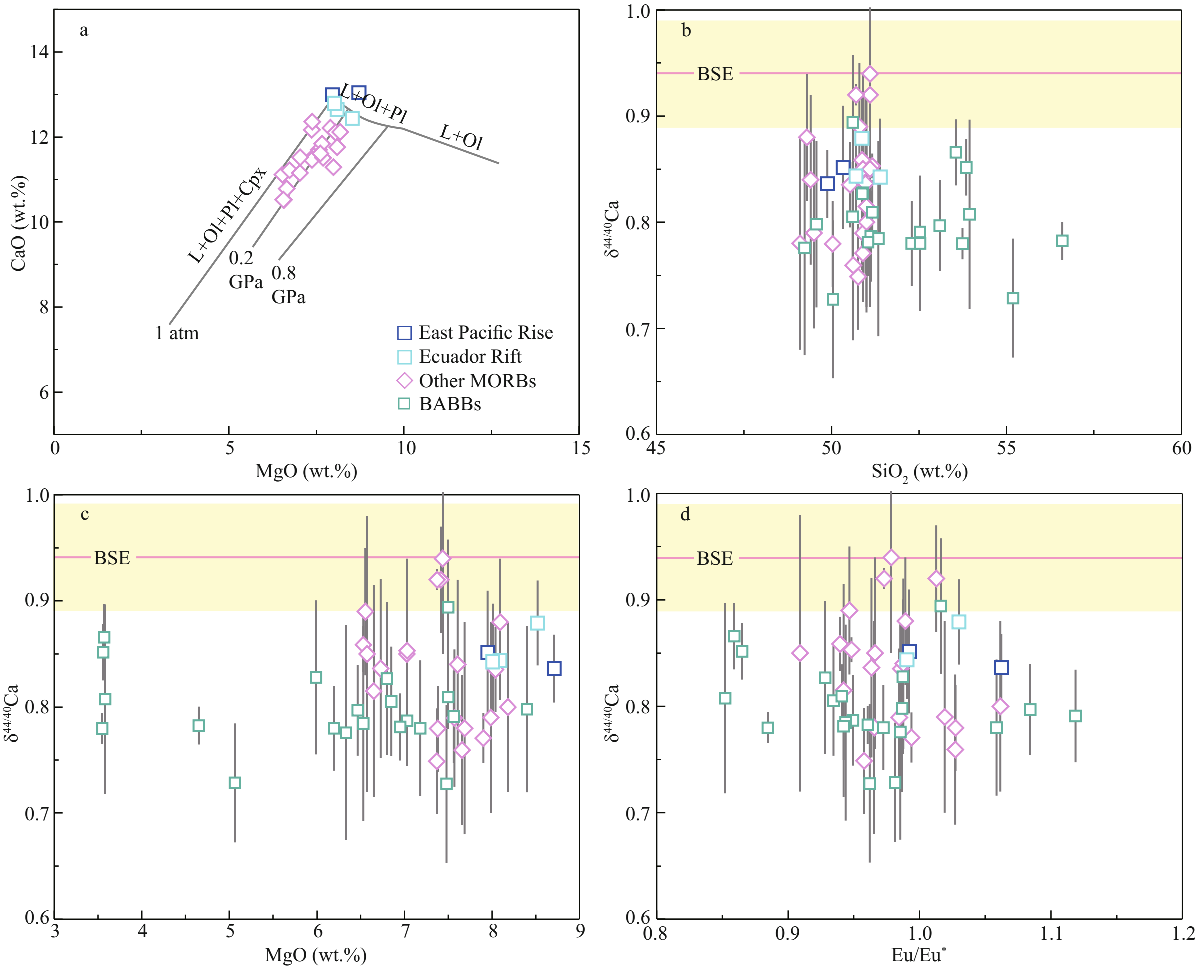

Fig.5 CaO content versus MgO content (a) and $\delta^{44/40}$Ca versus SiO_2 content (b), MgO contents (c), and Eu/Eu* (d) of studied MORB samples

Other MORB samples from the southern JdF Ridge, EPR and SMAR (Zhu et al., 2018b; Chen et al., 2019a), and BABB samples from the southwestern Pacific (Zhu et al., 2020a) are shown for comparison. The gray lines in panel a represent the crystallization sequence of primary MORB magma at three different pressures (101 325 Pa, 0.2 GPa, and 0.8 Gpa) calculated by Herzberg (2004). The pink vertical line and yellow bar represent the estimated $\delta^{44/40}$Ca value for the BSE (0.94‰±0.05‰; Kang et al., 2017).

5.3 The effect of fractional crystallization

Because of cooling at shallow levels, MORB samples are considered as residue melts that experienced fractional crystallization (Price et al., 1986; Smith et al., 1994; Niu, 1997). The sequence of fractional crystallization during isobaric magmatic differentiation at different pressures is: [L+Ol]→[L+Ol+Pl]→[L+Ol+Pl+Cpx] (Herzberg, 2004; Chen et al., 2019a). Our studied MORB samples display a limited variation in major element concentrations (Supplementary Table S1). The ranges of MgO and CaO concentrations suggest these MORB samples may experience fractional crystallization of Ol and Pl (Fig.5a).

Based on theoretical study, minerals with stronger bond strengths prefer heavier isotopes rather than the lighter ones (Urey, 1947). Due to the lower coordination numbers of Ca and shorter Ca-O bonds in Ol, this mineral with stronger bond strengths should be enriched in heavier Ca isotopes and have higher $\delta^{44/40}$Ca values than Cpx, which are consistent with experimental observations (Magna et al., 2015; Kang et al., 2016). However, as suggested by a simple balance calculation, Ol fractional crystallization cannot significantly affect Ca isotopic compositions of MORB samples (Zhu et al., 2018b). This is because the CaO contents in Ol (usually <0.4 wt.% in Ol; Sobolev et al., 2007) are too low to play an important role in lowering $\delta^{44/40}$Ca of the residual magmas (Liu et al., 2017a; Zhu et al., 2018b). Basaltic lavas from Hawaii with Ol accumulation have similar $\delta^{44/40}$Ca values to those of other basalts without Ol accumulation (Zhang et al., 2018), which further suggests that Ol fractional crystallization plays limited effects on $\delta^{44/40}$Ca of MORB samples.

Due to the high partition coefficient of Eu in Pl, Eu anomaly (defined as $Eu/Eu^*=w(Eu)_N/(w(Sm)_N\times w(Gd)_N)^{1/2}$, N refers to CI chondrite-normalized data that adopts from Sun and McDonough (1989)) can be used to assess the extent of Pl fractional crystallization (Nauret et al., 2006). MORB samples studied here do not display significant Eu anomaly with Eu/Eu* ranging from 0.99 to 1.06 (Fig.5d; Table 1), indicating these samples experienced less extent of Pl fractional crystallization. Moreover, Pl should not have higher $\delta^{44/40}$Ca values than the residue melt, as the Ca isotopic fractionation factor between Pl and basaltic melt ($\alpha_{\text{Pl-melt}}$) is slightly lower than 1 (Chen et al., 2019a). Thus, the lower $\delta^{44/40}$Ca of MORB samples compared to their mantle source cannot be caused by Pl fractional crystallization.

To further investigate the effect of magma differentiation on Ca isotopic fractionation, Chen et al. (2019a) made modelling calculations and found that the $\delta^{44/40}$Ca values of residual MORB melt are slightly higher (<0.05‰) than the primary melt. These results are consistent with the situation of our studied MORBs and reported MORBs and BABBs in literature (Zhu et al., 2018b, 2020a; Chen et al., 2019a), as their $\delta^{44/40}$Ca values do not show co-variations with SiO_2, MgO contents or Eu/Eu* (Fig.5b–d). Therefore, mafic magma differentiation cannot cause the lower $\delta^{44/40}$Ca signatures of our studied MORB samples.

5.4 The effect of mantle partial melting

The reported Ca isotopic signatures of mantle peridotites, MORBs and BABBs have demonstrated that Ca isotopic fractionation can occur during the process of mantle partial melting (Kang et al., 2017; Zhu et al., 2018b, 2020a; Chen et al., 2019a, b; Ionov et al., 2019). Specifically, melt-depleted lherzolites and harzburgites show gradually increased $\delta^{44/40}$Ca values (0.97‰–1.12‰) with their increasing degree of melt-extraction, and are systematically higher than those of the fertile peridotites that without modification by melting or metasomatism (Fig.3; Kang et al., 2017; Chen et al., 2019b; Ionov et al., 2019). Accordingly, the reported $\delta^{44/40}$Ca values of MORB samples range from 0.75‰ to 0.94‰ (Fig.3; Zhu et al., 2018b; Chen et al., 2019a), which are lower than their mantle source. Recently, Zhu et al. (2020a) observed that BABBs from the southwestern Pacific have lower $\delta^{44/40}$Ca values (0.73‰–0.89‰) than their mantle source (Fig.3), and proposed that the low $\delta^{44/40}$Ca signatures should be primarily controlled by Ca isotopic fractionation during partial melting without significant contributions from subducted materials.

In this study, MORB samples from the northeastern Pacific show narrow $\delta^{44/40}$Ca variations (0.84‰–0.88‰) with an average of 0.85‰±0.03‰, which is consistent with the averages of reported MORBs and BABBs within analytical uncertainty, but lower than that of the BSE and DMM (Fig.3). As discussed above, the low $\delta^{44/40}$Ca of studied MORBs cannot be attributed to seawater and/or hydrothermal alteration or fractional crystallization during magma differentiation. Therefore, mantle partial melting should be the primary factor that controls the Ca isotopic signatures of MORBs, and plausibly explains the offset of $\delta^{44/40}$Ca (~0.10‰) between the mantle and MORBs investigated here.

The behavior of Ca isotopes during partial melting is closely related to the inter-mineral Ca isotopic fractionation. For example, partial melts derived from eclogites are proposed to have lower $\delta^{44/40}$Ca than their sources, which should be caused by the Ca isotopic fractionation between garnet and Cpx (Kang et al., 2019; Wang et al., 2019). Generally, MORB samples are derived from mantle peridotites (Niu, 1997). Clinopyroxene, Opx and Ol are the major Ca-bearing minerals in mantle peridotites. Earlier studies have observed that Cpx has lower $\delta^{44/40}$Ca values than those of the coexisting Opx and Ol (Huang et al., 2010; Kang et al., 2016; Chen et al., 2019b). Melting experiments on mantle peridotites indicated that Cpx is consumed more rapidly than Opx in the residue during partial melting (Green, 1973; Jaques and Green, 1980). Thus, in the process of mantle partial melting, the light Ca isotopes from Cpx are preferentially incorporated into magma melt, while the heavy ones from Opx and Ol tend to stay in the residue. This mechanism can reasonably explain the lower $\delta^{44/40}$Ca signatures in MORBs and BABBs, and the higher $\delta^{44/40}$Ca signatures in melt-depleted peridotites (Fig.3; Kang et al., 2016, 2017; Zhu et al., 2018b, 2020a; Chen et al., 2019a; Ionov et al., 2019).

Several studies have made model calculations to further constrain the Ca isotopic fractionation during mantle partial melting (Zhang et al., 2018; Chen et al., 2019a; Zhu et al., 2020a). The results of these modelling calculations show that during mantle partial melting, the Ca isotopic fractionation factor between Opx and Cpx ($\alpha_{\text{Opx-Cpx}}$) has remarkable effect on $\delta^{44/40}$Ca of the melt. For instance, Zhang et al. (2018) found negligible effect (<0.04‰) on $\delta^{44/40}$Ca of the melt with $\alpha_{\text{Opx-Cpx}}$ ranging from 1.000 13 and 1.000 17. As $\alpha_{\text{Opx-Cpx}}$

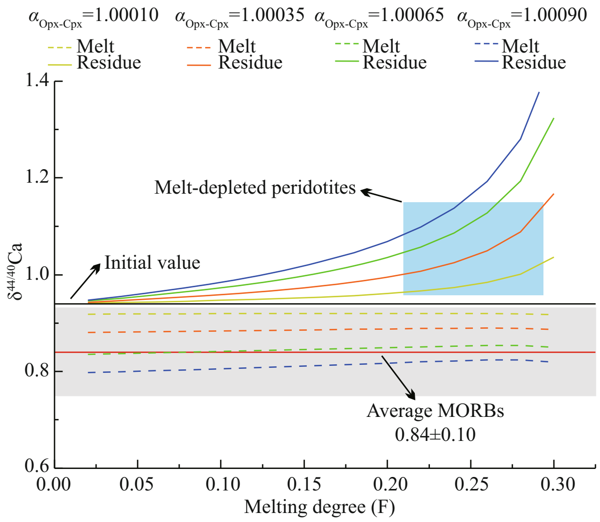

Fig.6 Incremental model of $\delta^{44/40}$Ca evolution during peridotite partial melting

The black horizontal line represents the starting peridotite with $\delta^{44/40}$Ca=0.94. The solid and dashed lines in different color represent modelling results for aggregate melts and incremental batch melting. The Ca isotopic fractionation factor between Cpx and basaltic melt ($\alpha_{Cpx-melt}$) is assumed to be 1 (Qi et al., 2017; Zhang et al., 2018; Chen et al., 2019b; Huang et al., 2019) and $\alpha_{Opx-Cpx}$ is assumed to vary between 1.000 10 and 1.000 90 based on the large range Ca isotopic fractionation between co-existing Opx and Cpx (Kang et al., 2016; Chen et al., 2019b). The red horizontal line and grey bar represent the average $\delta^{44/40}$Ca of our studied MORB and reported MORB samples (0.84‰±0.10‰). The blue area represents the range $\delta^{44/40}$Ca for melt-depleted peridotites (Kang et al., 2017; Ionov et al., 2019).

increases to 1.000 50, Chen et al. (2019b) found that $\delta^{44/40}$Ca of the melt can be 0.08‰ lower than that of the starting peridotite. The modelling results of aggregate melt with $\alpha_{Opx-Cpx}$=1.000 90 are 0.14‰ lower than that of the starting peridotite (Zhu et al., 2020a).

In this study, we performed modelling calculations and assumed $\alpha_{Cpx-melt}$=1 (Qi et al., 2017; Zhang et al., 2018; Chen et al., 2019b; Huang et al., 2019) and $\alpha_{Opx-Cpx}$ ranging from 1.000 1 to 1.000 9. Other parameters for the modelling are similar to those in Chen et al. (2019b) and Zhu et al. (2020a). Our modelling results of aggregate melt with $\alpha_{Opx-Cpx}$= 1.000 65 is consistent with the ~0.10‰ offset of $\delta^{44/40}$Ca between the BSE and the average of our studied MORB samples (Fig.6). These modelling results also show that the degrees of partial melting have limited effects of $\delta^{44/40}$Ca of aggregate melt (Fig.6).

Taken all the studied MORB samples together (Zhu et al., 2018b; Chen et al., 2019a), their $\delta^{44/40}$Ca values range from 0.75‰ to 0.94‰ with an average of 0.84‰±0.10‰ (2SD, *N*=26), which are 0–0.20‰ lower than the estimated value for the BSE. In addition to the minor effects of fractional crystallization, our modelling results show that the observed ~0.2‰ $\delta^{44/40}$Ca variation in these MORB samples from different locations may be related to the various Ca isotopic fractionation between Opx and Cpx in their mantle sources (Fig.6). Specifically, the $\Delta^{44/40}Ca_{Opx-Cpx}$ ($\Delta^{44/40}Ca_{Opx-Cpx}=\delta^{44/40}Ca_{Opx}-\delta^{44/40}Ca_{Cpx}$) in natural peridotites ranges from -0.01‰ to 1.29‰, which are dominated by the Ca/Mg ratios in Opx and temperature (Kang et al., 2016; Wang et al., 2017; Chen et al., 2019b). During partial melting, mantle peridotites with different $\alpha_{Opx-Cpx}$ can be one of the factors that induce various $\delta^{44/40}$Ca in MORB samples. Moreover, the heterogeneity of mantle sources may also play a role in causing the $\delta^{44/40}$Ca variation in MORB samples, as low proportion of pyroxenites are proposed to exist in their mantle sources (Sobolev et al., 2007).

6 CONCLUSION

Calcium isotopic compositions of D-MORB samples from the East Pacific Rise and Ecuador Rift in the northeastern Pacific have been studied here to constrain the Ca isotopic fractionation during mantle partial melting. The $\delta^{44/40}$Ca of these MORB samples display little variations from 0.84‰ to 0.88‰ with an average of 0.85‰±0.03‰, which is consistent with the averages of reported MORBs and BABBs within uncertainty, but is ~0.10‰ lower than that of the BSE and DMM. Seawater and hydrothermal alteration and fractional crystallization were excluded for explaining the low $\delta^{44/40}$Ca signatures of MORB samples. Instead, the ~0.10‰ offset of $\delta^{44/40}$Ca between MORBs and the BSE is most likely caused by mantle partial melting. During this process, the light Ca isotopes are preferred to be enriched in magma melt, while the heavy ones tend to stay in the residue, which is in accordance with the fact that $\delta^{44/40}$Ca of melt-depleted peridotites increases with partial melting in literature. Therefore, mantle partial melting should be considered as one of the important processes for causing the Ca isotopic heterogeneity in Earth's mantle.

7 DATA AVAILABILITY STATEMENT

All data generated and/or analyzed during this study are available from the corresponding author upon reasonable request.

8 ACKNOWLEDGMENT

We are extremely grateful to LIU Fang, KANG Jinting, and LIU Yufei for help in sample analysis and discussion. We are also grateful to the editors and the anonymous reviewers, whose constructive suggestions greatly improved our manuscript.

References

Amini M, Eisenhauer A, Böhm F, Fietzke J, Bach W, Garbe-Schönberg D, Rosner M, Bock B, Lackschewitz K S, Hauff F. 2008. Calcium isotope ($\delta^{44/40}$Ca) fractionation along hydrothermal pathways, Logatchev field (Mid-Atlantic Ridge, 14°45′N). *Geochimica et Cosmochimica Acta*, **72**(16): 4 107-4 122.

Amini M, Eisenhauer A, Böhm F, Holmden C, Kreissig K, Hauff F, Jochum K P. 2009. Calcium Isotopes ($\delta^{44/40}$Ca) in MPI-DING reference glasses, USGS rock powders and various rocks: evidence for Ca isotope fractionation in terrestrial silicates. *Geostandards and Geoanalytical Research*, **33**(2): 231-247.

Amsellem E, Moynier F, Pringle E A, Bouvier A, Chen H, Day J M D. 2017. Testing the chondrule-rich accretion model for planetary embryos using calcium isotopes. *Earth and Planetary Science Letters*, **469**: 75-83.

Amsellem E, Moynier F, Puchtel I S. 2019. Evolution of the Ca isotopic composition of the mantle. *Geochimica et Cosmochimica Acta*, **258**: 195-206.

Antonelli M A, Mittal T, McCarthy A, Tripoli B, Watkins J M, DePaolo D J. 2019a. Ca isotopes record rapid crystal growth in volcanic and subvolcanic systems. *Proceedings of the National Academy of Sciences of the United States of America*, **116**(41): 20 315-2 0321.

Antonelli M A, Schiller M, Schauble E A, Mittal T, DePaolo D J, Chacko T, Grew E S, Tripoli B. 2019b. Kinetic and equilibrium Ca isotope effects in high-T rocks and minerals. *Earth and Planetary Science Letters*, **517**: 71-82.

Blättler C L, Higgins J A. 2017. Testing Urey's carbonate-silicate cycle using the calcium isotopic composition of sedimentary carbonates. *Earth and Planetary Science Letters*, **479**: 241-251.

Charlier B L A, Ginibre C, Morgan D, Nowell G M, Pearson D G, Davidson J P, Ottley C J. 2006. Methods for the microsampling and high-precision analysis of strontium and rubidium isotopes at single crystal scale for petrological and geochronological applications. *Chemical Geology*, **232**(3-4): 114-133.

Chen C F, Ciazela J, Li W, Dai W, Wang Z C, Foley S F, Li M, Hu Z C, Liu Y S. 2019a. Calcium isotopic compositions of oceanic crust at various spreading rates. *Geochimica et Cosmochimica Acta*, https://doi.org/10.1016/j.gca.2019. 07.008.

Chen C F, Dai W, Wang Z C, Liu Y S, Li M, Becker H, Foley S F. 2019b. Calcium isotope fractionation during magmatic processes in the upper mantle. *Geochimica et Cosmochimica Acta*, **249**: 121-137.

Chen C F, Liu Y S, Feng L P, Foley S F, Zhou L, Ducea M N, Hu Z C. 2018. Calcium isotope evidence for subduction-enriched lithospheric mantle under the northern North China Craton. *Geochimica et Cosmochimica Acta*, **238**: 55-67.

Dai W, Wang Z C, Liu Y S, Chen C F, Zong K Q, Zhou L, Zhang G L, Li M, Moynier F, Hu Z C. 2020. Calcium isotope compositions of mantle pyroxenites. *Geochimica et Cosmochimica Acta*, **270**: 144-159.

DePaolo D J. 2004. Calcium isotopic variations produced by biological, kinetic, radiogenic and nucleosynthetic processes. *Reviews in Mineralogy and Geochemistry*, **55**(1): 255-288.

Du L, Long X P, Yuan C, Zhang Y Y, Huang Z Y, Sun M, Xiao W J. 2018. Petrogenesis of Late Paleozoic diorites and A-type granites in the central Eastern Tianshan, NW China: response to post-collisional extension triggered by slab breakoff. *Lithos*, **318-319**: 47-59.

Du L, Yuan C, Li X P, Zhang Y Y, Huang Z Y, Long X P. 2019a. Petrogenesis and geodynamic implications of the carboniferous Granitoids in the Dananhu Belt, Eastern Tianshan Orogenic Belt. *Journal of Earth Science*, **30**(6): 1 243-1 252.

Du L, Zhang Y Y, Huang Z Y, Li X P, Yuan C, Wu B, Long X P. 2019b. Devonian to carboniferous tectonic evolution of the Kangguer Ocean in the Eastern Tianshan, NW China: insights from three episodes of granitoids. *Lithos*, **350-351**: 105243.

Fantle M S, Tipper E T. 2014. Calcium isotopes in the global biogeochemical Ca cycle: implications for development of a Ca isotope proxy. *Earth-Science Reviews*, **129**: 148-177.

Farkaš J, Böhm F, Wallmann K, Blenkinsop J, Eisenhauer A, Van Geldern R, Munnecke A, Voigt S, Veizer J. 2007a. Calcium isotope record of Phanerozoic oceans: implications for chemical evolution of seawater and its causative mechanisms. *Geochimica et Cosmochimica Acta*, **71**(21): 5 117-5 134.

Farkaš J, Buhl D, Blenkinsop J, Veizer J. 2007b. Evolution of the oceanic calcium cycle during the late Mesozoic: evidence from $\delta^{44/40}$Ca of marine skeletal carbonates. *Earth and Planetary Science Letters*, **253**(1-2): 96-111.

Feng C Q, Qin T, Huang S C, Wu Z Q, Huang F. 2014. First-principles investigations of equilibrium calcium isotope fractionation between clinopyroxene and Ca-doped orthopyroxene. *Geochimica et Cosmochimica Acta*, **143**: 132-142.

Feng L P, Zhou L, Yang L, DePaolo D J, Tong S Y, Liu Y S, Owens T L, Gao S. 2017. Calcium isotopic compositions of sixteen USGS reference materials. *Geostandards and Geoanalytical Research*, **41**(1): 93-106.

Feng L P, Zhou L, Yang L, Zhang W, Wang Q, Tong S Y, Hu Z C. 2018. A rapid and simple single-stage method for Ca separation from geological and biological samples for isotopic analysis by MC-ICP-MS. *Journal of Analytical Atomic Spectrometry*, **33**(3): 413-421.

Gale A, Dalton C A, Langmuir C H, Su Y J, Schilling J G. 2013. The mean composition of ocean ridge basalts. *Geochemistry*, *Geophysics*, *Geosystems*, **14**(3): 489-518.

Green D H. 1973. Experimental melting studies on a model upper mantle composition at high pressure under water-saturated and water-undersaturated conditions. *Earth and Planetary Science Letters*, **19**(1): 37-53.

He Y S, Wang Y, Zhu C W, Huang S C, Li S G. 2017. Mass-independent and mass-dependent Ca Isotopic compositions of thirteen geological reference materials measured by thermal Ionisation mass spectrometry. *Geostandards and*

Geoanalytical Research, **41**(2): 283-302.

Herzberg C. 2004. Partial crystallization of Mid-Ocean Ridge Basalts in the crust and mantle. *Journal of Petrology*, **45**(12): 2 389-2 405.

Heuser A, Eisenhauer A, Gussone N, Bock B, Hansen B T, Nägler T F. 2002. Measurement of calcium isotopes (δ^{44}Ca) using a multicollector TIMS technique. *International Journal of Mass Spectrometry*, **220**(3): 385-397.

Huang F, Zhou C, Wang W Z, Kang J T, Wu Z Q. 2019. First-principles calculations of equilibrium Ca isotope fractionation: implications for oldhamite formation and evolution of lunar magma ocean. *Earth and Planetary Science Letters*, **510**: 153-160.

Huang S C, Farkaš J, Jacobsen S B. 2010. Calcium isotopic fractionation between clinopyroxene and orthopyroxene from mantle peridotites. *Earth and Planetary Science Letters*, **292**(3-4): 337-344.

Huang S C, Farkaš J, Jacobsen S B. 2011. Stable calcium isotopic compositions of Hawaiian shield lavas: evidence for recycling of ancient marine carbonates into the mantle. *Geochimica et Cosmochimica Acta*, **75**(17): 4 987-4 997.

Huang S C, Jacobsen S B. 2017. Calcium isotopic compositions of chondrites. *Geochimica et Cosmochimica Acta*, **201**: 364-376.

Ionov D A, Qi Y H, Kang J T, Golovin A V, Oleinikov O B, Zheng W, Anbar A D, Zhang Z F, Huang F. 2019. Calcium isotopic signatures of carbonatite and silicate metasomatism, melt percolation and crustal recycling in the lithospheric mantle. *Geochimica et Cosmochimica Acta*, **248**: 1-13.

Jaques A L, Green D H. 1980. Anhydrous melting of peridotite at 0-15 kb pressure and the genesis of tholeiitic basalts. *Contributions to Mineralogy and Petrology*, **73**(3): 287-310.

John T, Gussone N, Podladchikov Y Y, Bebout G E, Dohmen R, Halama R, Klemd R, Magna T, Seitz H M. 2012. Volcanic arcs fed by rapid pulsed fluid flow through subducting slabs. *Nature Geoscience*, **5**(7): 489-492.

Kang J T, Ionov D A, Liu F, Zhang C L, Golovin A V, Qin L P, Zhang Z F, Huang F. 2017. Calcium isotopic fractionation in mantle peridotites by melting and metasomatism and Ca isotope composition of the Bulk Silicate Earth. *Earth and Planetary Science Letters*, **474**: 128-137.

Kang J T, Ionov D A, Zhu H L, Liu F, Zhang Z F, Liu Z, Huang F. 2019. Calcium isotope sources and fractionation during melt-rock interaction in the lithospheric mantle: evidence from pyroxenites, wehrlites, and eclogites. *Chemical Geology*, **524**: 272-282.

Kang J T, Zhu H L, Liu Y F, Liu F, Wu F, Hao Y T, Zhi X C, Zhang Z F, Huang F. 2016. Calcium isotopic composition of mantle xenoliths and minerals from Eastern China. *Geochimica et Cosmochimica Acta*, **174**: 335-344.

Li M, Lei Y, Feng L P, Wang Z C, Belshaw N S, Hu Z C, Liu Y S, Zhou L, Chen H H, Chai X N. 2018. High-precision Ca isotopic measurement using a large geometry high resolution MC-ICP-MS with a dummy bucket. *Journal of Analytical Atomic Spectrometry*, **33**(10): 1 707-1 719.

Liu F, Li X, An Y J, Li J, Zhang Z F. 2019. Calcium isotope ratio ($\delta^{44/40}$Ca) measurements of Ca-dominated minerals and rocks without column chemistry using the double-spike technique and thermal ionisation mass spectrometry. *Geostandards and Geoanalytical Research*, **43**(3): 509-517.

Liu F, Li X, Wang G Q, Liu Y F, Zhu H L, Kang J T, Huang F, Sun W D, Xia X P, Zhang Z F. 2017a. Marine carbonate component in the mantle beneath the southeastern Tibetan Plateau: evidence from magnesium and calcium isotopes. *Journal of Geophysical Research*: *Solid Earth*, **122**: 9 729-9 744.

Liu F, Zhang Z F, Li X, An Y J. 2020. A practical guide to the double-spike technique for calcium isotope measurements by Thermal Ionization Mass Spectrometry (TIMS). *International Journal of Mass Spectrometry*, **450**: 116307.

Liu F, Zhu H L, Li X, Wang G Q, Zhang Z F. 2017b. Calcium isotopic fractionation and compositions of geochemical reference materials. *Geostandards and Geoanalytical Research*, **41**(4): 675-688.

Lu W N, He Y S, Wang Y, Ke S. 2019. Behavior of calcium isotopes during continental subduction recorded in meta-basaltic rocks. *Geochimica et Cosmochimica Acta*, https://doi.org/10.1016/j.gca.2019.09.027.

Lundstrom C C, Sampson D E, Perfit M R, Gill J, Williams Q. 1999. Insights into mid-ocean ridge basalt petrogenesis: u-series disequilibria from the Siqueiros Transform, Lamont Seamounts, and East Pacific Rise. *Journal of Geophysical Research*, **104**(B3): 13 035-13 048.

Ma J L, Wei G J, Liu Y, Ren Z Y, Xu Y G, Yang Y H. 2013. Precise measurement of stable neodymium isotopes of geological materials by using MC-ICP-MS. *Journal of Analytical Atomic Spectrometry*, **28**(12): 1 926-1 931.

Magna T, Gussone N, Mezger K. 2015. The calcium isotope systematics of Mars. *Earth and Planetary Science Letters*, **430**: 86-94.

Nauret F, Abouchami W, Galer S J G, Hofmann A W, Hémond C, Chauvel C, Dyment J. 2006. Correlated trace element-Pb isotope enrichments in Indian MORB along 18-20°S, Central Indian Ridge. *Earth and Planetary Science Letters*, **245**(1-2): 137-152.

Niu Y L. 1997. Mantle melting and melt extraction processes beneath ocean ridges: evidence from abyssal peridotites. *Journal of Petrology*, **38**(8): 1 047-1 074.

Perfit M R, Fornari D J, Malahoff A, Embley R W. 1983. Geochemical studies of abyssal lavas recovered by DSRV *Alvin* from Eastern Galapagos Rift, Inca Transform, and Ecuador Rift: 3. Trace element abundances and petrogenesis. *Journal of Geophysical Research*: *Solid Earth*, **88**(B12): 10 551-10 572.

Price R C, Kennedy A K, Riggs-Sneeringer M, Frey F A. 1986. Geochemistry of basalts from the Indian Ocean triple junction: implications for the generation and evolution of Indian Ocean ridge basalts. *Earth and Planetary Science Letters*, **78**(4): 379-396.

Qi Y H, Liu X H, Kang J T, He L X. 2017. First-principles investigations of equilibrium Ca, Mg, Si and O isotope fractionations between silicate melts and minerals. *In*: Proceedings of AGU Fall Meeting Abstracts. American Geophysical Union, New Orleans.

Raczek I, Jochum K P, Hofmann A W. 2003. Neodymium and strontium isotope data for USGS reference materials BCR-1, BCR-2, BHVO-1, BHVO-2, AGV-1, AGV-2, GSP-1, GSP-2 and eight MPI-DING reference glasses. *Geostandards Newsletter*, **27**(2): 173-179.

Richter F M, Dauphas N, Teng F Z. 2009. Non-traditional fractionation of non-traditional isotopes: evaporation, chemical diffusion and Soret diffusion. *Chemical Geology*, **258**(1-2): 92-103.

Salters V J M, Stracke A. 2004. Composition of the depleted mantle. *Geochemistry*, *Geophysics*, *Geosystems*, **5**(5): Q05B07.

Simon J I, DePaolo D J. 2010. Stable calcium isotopic composition of meteorites and rocky planets. *Earth and Planetary Science Letters*, **289**(3-4): 457-466.

Skulan J, DePaolo D J, Owens T L. 1997. Biological control of calcium isotopic abundances in the global calcium cycle. *Geochimica et Cosmochimica Acta*, **61**(12): 2 505-2 510.

Smith M C, Perfit M R, Jonasson I R. 1994. Petrology and geochemistry of basalts from the southern Juan de Fuca Ridge: controls on the spatial and temporal evolution of mid-ocean ridge basalt. *Journal of Geophysical Research*: *Solid Earth*, **99**(3): 4 787-4 812.

Sobolev A V, Hofmann A W, Kuzmin D V, Yaxley G M, Arndt N T, Chung S L, Danyushevsky L V, Elliott T, Frey F A, Garcia M O, Gurenko A A, Kamenetsky V S, Kerr A C, Krivolutskaya N A, Matvienkov V V, Nikogosian I K, Rocholl A, Sigurdsson I A, Sushchevskaya N M, Teklay M. 2007. The amount of recycled crust in sources of mantle-derived melts. *Science*, **316**(5823): 412-417.

Sun S S, McDonough W F. 1989. Chemical and isotopic systematics of oceanic basalts: implications for mantle composition and processes. *Geological Society*, *London*, *Special Publications*, **42**(1): 313-345.

Sun W, Bennett V C, Eggins S M, Arculus R J, Perfit M R. 2003. Rhenium systematics in submarine MORB and back-arc basin glasses: laser ablation ICP-MS results. *Chemical Geology*, **196**(1-4): 259-281.

Tanaka T, Togashi S, Kamioka H, Amakawa H, Kagami H, Hamamoto T, Yuhara M, Orihashi Y, Yoneda S, Shimizu H, Kunimaru T, Takahashi K, Yanagi T, Nakano T, Fujimaki H, Shinjo R, Asahara Y, Tanimizu M, Dragusanu C. 2000. JNdi-1: a neodymium isotopic reference in consistency with LaJolla neodymium. *Chemical Geology*, **168**(3-4): 279-281.

Thirlwall M F. 1991. Long-term reproducibility of multicollector Sr and Nd isotope ratio analysis. *Chemical Geology*: *Isotope Geoscience section*, **94**(2): 85-104.

Urey H C. 1947. The thermodynamic properties of isotopic substances. *Journal of the Chemical Society* (*Resumed*), **562**: 562-581.

Valdes M C, Debaille V, Berger J, Armytage R M G. 2019. The effects of high-temperature fractional crystallization on calcium isotopic composition. *Chemical Geology*, **509**: 77-91.

Valdes M C, Moreira M, Foriel J, Moynier F. 2014. The nature of Earth's building blocks as revealed by calcium isotopes. *Earth and Planetary Science Letters*, **394**: 135-145.

Verma S P. 1992. Seawater alteration effects on REE, K, Rb, Cs, Sr, U, Th, Pb and Sr-Nd-Pb isotope systematics of Mid-Ocean Ridge Basalt. *Geochemical Journal*, **26**(3): 159-177.

Wang W Z, Zhou C, Qin T, Kang J T, Huang S C, Wu Z Q, Huang F. 2017. Effect of Ca content on equilibrium Ca isotope fractionation between orthopyroxene and clinopyroxene. *Geochimica et Cosmochimica Acta*, **219**: 44-56.

Wang Y, He Y S, Wu H J, Zhu C W, Huang S C, Huang J. 2019. Calcium isotope fractionation during crustal melting and magma differentiation: granitoid and mineral-pair perspectives. *Geochimica et Cosmochimica Acta*, **259**: 37-52.

Workman R K, Hart S R. 2005. Major and trace element composition of the depleted MORB mantle (DMM). *Earth and Planetary Science Letters*, **231**(1-2): 53-72.

Wu W, Xu Y G, Zhang Z F, Li X. 2020. Calcium isotopic composition of the lunar crust, mantle, and bulk silicate Moon: a preliminary study. *Geochimica et Cosmochimica Acta*, **270**: 313-324.

Zhang H M, Wang Y, He Y S, Teng F Z, Jacobsen S B, Helz R T, Marsh B D, Huang S C. 2018. No measurable calcium isotopic fractionation during crystallization of Kilauea Iki lava lake. *Geochemistry*, *Geophysics*, *Geosystems*, **19**(9): 3 128-3 139.

Zhao X M, Zhang Z F, Huang S C, Liu Y F, Li X, Zhang H F. 2017. Coupled extremely light Ca and Fe isotopes in peridotites. *Geochimica et Cosmochimica Acta*, **208**: 368-380.

Zhu H L, Du L, Li X, Zhang Z F, Sun W D. 2020a. Calcium isotopic fractionation during plate subduction: constraints from back-arc basin basalts. *Geochimica et Cosmochimica Acta*, **270**: 379-393.

Zhu H L, Liu F, Li X, An Y J, Nan X Y, Du L, Huang F, Sun W D, Zhang Z F. 2020b. Significant $\delta^{44/40}$Ca variations between carbonate- and clay-rich marine sediments from the Lesser Antilles forearc and implications for mantle heterogeneity. *Geochimica et Cosmochimica Acta*, **276**: 239-257.

Zhu H L, Liu F, Li X, An Y J, Wang G Q, Zhang Z F. 2018a. A "peak cut" procedure of column separation for calcium isotope measurement using the double spike technique and Thermal Ionization Mass Spectrometry (TIMS). *Journal of Analytical Atomic Spectrometry*, **33**(4): 547-554.

Zhu H L, Liu F, Li X, Wang G Q, Zhang Z F, Sun W D. 2018b. Calcium isotopic compositions of normal Mid-Ocean Ridge Basalts from the southern Juan de Fuca Ridge. *Journal of Geophysical Research*: *Solid Earth*, **123**(2): 1 303-1 313.

Zhu H L, Zhang Z F, Wang G Q, Liu Y F, Liu F, Li X, Sun W D. 2016. Calcium isotopic fractionation during ion-exchange column chemistry and Thermal Ionisation Mass Spectrometry (TIMS) determination. *Geostandards and Geoanalytical Research*, **40**(2): 185-194.

Electronic supplementary material

Supplementary material (Supplementary Table S1) is available in the online version of this article at https://doi.org/10.1007/s00343-020-0045-2.